Localization-driven correlated states of two isolated interacting helical edges

Yang-Zhi Chou

Phys. Rev. B **99**, 045125 — Published 14 January 2019

DOI: 10.1103/PhysRevB.99.045125

Localization-Driven Correlated States of Two Isolated Interacting Helical Edges

Yang-Zhi Chou*
Department of Physics and Center for Theory of Quantum Matter, University of Colorado Boulder, Boulder, Colorado 80309, USA
(Dated: November 28, 2018)

We study the *localization-driven* correlated states among two isolated dirty interacting helical edges as realized at the boundaries of two-dimensional $\mathbb{Z}_2$ topological insulators. We show that an interplay of time-reversal symmetric disorder and strong inter-edge interactions generically drives the entire system to a gapless localized state, preempting all other intra-edge instabilities. For weaker interactions, an anti-symmetric interlocked fluid, causing a negative perfect drag, can emerge from dirty edges with different densities. We also find that the interlocked fluid states of helical edges are stable against the leading intra-edge perturbation down to zero temperature. The corresponding experimental signatures including zero temperature and finite temperature transport are discussed.

I. INTRODUCTION

Quenched randomness (disorder) can drastically suppress the electronic transport by inducing Anderson localization[1], a phenomena that is known to be prominent in low dimensions. Cooperations of interaction and disorder can induce manybody localization[2–4] which exhibits ergodicity breaking and enables unexpected orders[5]. As a striking outcome, a combination of time-reversal (TR) symmetric disorder and inter-particle interactions can drive a two-dimensional (2D) topological insulator[6–11] (TI) edge, conducting ballistically in the absence of interaction[6,12], to a gapless insulating edge[13]. In this work, we further explore the new correlated states due to a similar *localizing* mechanism among two isolated interacting $\mathbb{Z}_2$ TI edges with quenched disorder.

A 2D TR symmetric TI[6–11] is a fully gapped bulk insulator whose edge is described by counter-propagating electrons forming Kramers pairs. The TR symmetry prevents the edge electrons from Anderson localization which generically ceases conductions in the conventional one-dimensional systems. Such a topological protected state emerges a helical Luttinger liquid description[14,15] and exhibits a quantized e^2/h edge conductance at zero temperature. The possibility of realizing 2D TR symmetric TI motivates various experimental studies[16–30] which might pave the way for creating Majorana and $\mathbb{Z}_4$ parafermion zero modes, enabling topological quantum computations[31–34].

Contrary to the well-studied single edge problems (see recent reviews[35,36] and the references therein), the physics of two interacting TI edges[37–43] has not been explored systematically, the effect due to simultaneous appearance of disorder and interactions especially. In this work, we focus on the low temperature regimes of two isolated dirty interacting TI edges with different densities. We show that the combinations of inter-edge interactions and disorder can generate new types of localization-driven correlated states: A gapless insulating state with both edges being spontaneously TR symmetry broken, and an anti-symmetric interlocked fluid with edges carrying opposite currents. The former represents an inter-edge instability that preempts all other phases driven by TR symmetric intra-edge perturbations. The latter corresponds to a zero temperature perfect *negative drag* in striking contrast with the well known perfect positive drag among quantum wires[44,45]. These regimes are summarized in Fig. 1. We also discuss the stability of the negative drag state against intra-edge perturbation. Both of the inter-edge correlated states can be measured via a specific Coulomb drag[46,47] related experimental setup[39] as illustrated in Fig. 2 (a). Concomitantly, we predict the two terminal conductance at zero temperature (Fig. 3) and finite temperatures (Fig. 4).

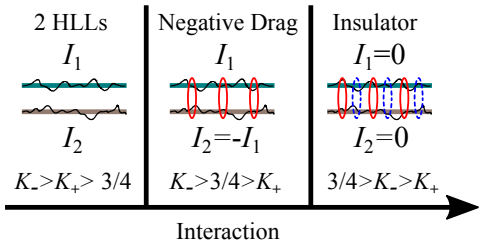

FIG. 1. Zero temperature phase diagram of two dirty TI edges with different densities. We assume $1 > K_- > K_+$ due to the repulsive interactions. For $K_- > K_+ > 3/4$, the two helical Luttinger liquids are decoupled. The symmetric inter-edge mode is localized when $K_- > 3/4 > K_+$. An anti-symmetric interlocked fluid is developed. For $3/4 > K_- > K_+$, the a gapless localized insulator is predicted.

II. MODEL

We consider two isolated TR symmetric $\mathbb{Z}_2$ TI edges that interact via Coulomb force[37–39,42] but do not allow inter-edge electron tunnelings. For each isolated edge, there are counter-propagating right (R) and left (L) mover fermions forming Kramers pairs. In the low energy limit, the kinetic term is given by

$$\hat{H}_0 = -i \sum_{a=1,2} v_{Fa} \int dx \left[R_a^\dagger(x) \partial_x R_a(x) - L_a^\dagger(x) \partial_x L_a(x) \right], \tag{1}$$

where $a = 1, 2$ is the edge index and v_{Fa} is the Fermi velocity of the ath edge band. Time-reversal operation is encoded by $R_a(x) \to L_a(x)$, $L_a(x) \to -R_a(x)$, and $i \to -i$. Therefore, the conventional backscattering (e.g., $R^\dagger L + L^\dagger R$ in the spinless Luttinger liquid) is prohibited[6]. The time-reversal symmetric disorder is the chemical potential fluctuation (pure forward scattering) given by,

$$\hat{H}_V = \sum_{a=1,2} \int dx\, V_a(x) \left[R_a^\dagger(x) R_a(x) + L_a^\dagger(x) L_a(x) \right], \quad (2)$$

where $V_a(x)$ is the disordered potential in the ath edge. We assume that the disordered potentials are zero-mean Gaussian random variables and satisfy $\overline{V_a(x) V_b(y)} = \Delta \delta_{ab} \delta(x-y)$, where $\overline{\mathcal{O}}$ denotes a disorder average of $\mathcal{O}$.

The interaction between the two helical edges is primarily due to Coulomb interaction. Instead of studying specific microscopic models, we construct the inter-edge perturbations via symmetry and relevance in the renormalization group analysis. The leading TR symmetric backscattering terms are the inter-edge umklapp interactions[37,39] given by

$$\hat{H}_{U,+} = U_+ \int dx \left[e^{-i\delta Q_+ x} L_1^\dagger R_1 L_2^\dagger R_2 + \text{H.c.} \right], \quad (3)$$

$$\hat{H}_{U,-} = U_- \int dx \left[e^{-i\delta Q_- x} L_1^\dagger R_1 R_2^\dagger L_2 + \text{H.c.} \right]. \quad (4)$$

In the above equations, $\delta Q_\pm = Q_\pm - 2(k_{F1} \pm k_{F2})$ measures the lack of commensuration, $Q_\pm = 2\pi/d$ is the commensuration wavevector (d is the lattice constant of the 2D bulk), and k_{F1} (k_{F2}) indicates the Fermi wavevector in the first (second) edge. Generically, both $\hat{H}_{U,-}$ and $\hat{H}_{U,+}$ are irrelevant due to incommensuration. We ignore the intra-edge backscattering terms since they are subleading[39,48,49].

In order to include Luttinger liquid effects (arising from both intra- and inter-edge interactions), we use standard bosonization[50,51]. The density (n_a) and current (I_a) can be expressed in terms of the phonon-like field (θ_a). $n_a = \partial_x \theta_a / \pi$ and $I_a = -\partial_t \theta_a / \pi$. The two helical Luttinger liquids problem can be decomposed into symmetric and anti-symmetric inter-edge degrees of freedom. In the imaginary time path integral, the bosonic action[37,39,45] is given by $\mathcal{S}_\pm = \mathcal{S}_{0,\pm} + \mathcal{S}_{V,\pm} + \mathcal{S}_{U,\pm}$, where

$$\mathcal{S}_{0,\pm} = \frac{1}{2\pi v_\pm K_\pm} \int d\tau dx \, \left[(\partial_\tau \Theta_\pm)^2 + v_\pm^2 (\partial_x \Theta_\pm)^2 \right], \quad (5a)$$

$$\mathcal{S}_{V,\pm} = \int d\tau dx\, V_\pm(x) \frac{1}{\pi} \partial_x \Theta_\pm, \quad (5b)$$

$$\mathcal{S}_{U,\pm} = \frac{U_\pm}{2\pi^2 \alpha^2} \int d\tau dx \, \cos\left[2\sqrt{2} \Theta_\pm - \delta Q_\pm x \right], \quad (5c)$$

where $\Theta_\pm = \frac{1}{\sqrt{2}} [\theta_1 \pm \theta_2]$ encodes the symmetric (+) and anti-symmetric (−) collective modes, $K_\pm$ ($v_\pm$) is the Luttinger parameter (velocity), $V_\pm(x) = \frac{1}{\sqrt{2}} [V_1(x) \pm V_2(x)]$ is the disorder potential, and α is an ultraviolet length scale.

The inter-edge Luttinger interaction is given by $(\partial_x \theta_1)(\partial_x \theta_2) \propto (\partial_x \Theta_+)(\partial_x \Theta_+) - (\partial_x \Theta_-)(\partial_x \Theta_-)$. As a consequence, repulsive inter-edge interactions tend to decrease K_+ and increase K_-. [Note that $K_\pm < 1$ ($K_\pm > 1$) for overall repulsive (attractive) interactions.] Importantly, the intra-edge Luttinger interactions still dominate and drive $K_\pm < 1$[45]. We therefore assume that $1 > K_- > K_+$ holds generically.

Lastly, we discuss the disorder terms. $V_\pm(x)$ is a Gaussian random field which obeys $\overline{V_\pm(x)} = 0$, $\overline{V_\pm(x) V_\pm(y)} = \Delta \delta(x-y)$, and $\overline{V_+(x) V_-(y)} = 0$. The above conditions ensure that the symmetric and anti-symmetric sectors are completely decoupled. The intra-edge perturbation will hybridize the two sectors. We will discuss the validity of our model in the end of the next section.

III. LOCALIZATION-DRIVEN CORRELATED STATE

We now discuss the zero temperature states in the simultaneously appearance of the inter-edge backscattering and the TR symmetric disorder. We will first review the mechanism that drives inter-edge collective modes into localization. Two new states (inter-edge localized and interlocked fluid states) can be inferred from the localization physics. We finally discuss the stability of the interlocked fluid states against intra-edge perturbations.

A. Interplay of disorder and interaction

The two helical Lutinger liquids problem can be viewed as two decoupled problems of a disordered interacting helical edge[13] with proper rescaling of parameters. We briefly review the ideas in Ref. 13 and discuss the localization physics in this subsection.

We first discuss the stability of the Luttinger liquid phase. The disorder potential $\mathcal{S}_{V,\pm}$ [given by Eq. (5b)] generates chemical potential spatial fluctuations but does not induce backscattering. On the other hand, the inter-edge umklapp backscattering interaction $\mathcal{S}_{U,\pm}$ [given by Eq. (5c)] alone cannot gap out $\Theta_\pm$ unless $|\delta Q_\pm| \le \delta Q_c$[52] (where δQ_c is the critical value in the commensurate-incommensurate transition). Therefore, the Luttinger liquid phase is generically stable with only disorder or interaction. Nevertheless, the fluctuations of chemical potentials (equivalent to the fluctuations of k_{F1} and k_{F2}) compensate the *missing* momenta ($\delta Q_\pm$) in a random fashion. As a result, the backscattering is enhanced due to "local commensuration"[13,39,49,53]. Both the symmetric and anti-symmetric sectors in Eq. (5) can be mapped to the localization problem studied in Ref. 13 with a rescaling $K \to K_\pm/2$. The critical value $K_\pm = 3/4$[54] (less interacting than the single edge critical value $K =$

$3/8$[13–15]) separates a Luttinger liquid phase and a gapless localized phase.

For sufficiently strong interactions ($K_\pm < 3/4$), the inter-edge $\Theta_\pm$ sector is driven to a localized state[13,55,56] as the full gapped state (due to $\mathcal{S}_{U,\pm}$) is not stable against the *random field* disorder given by $\mathcal{S}_{V,\pm}$[13,57]. In addition, the bosonized theory at $K_\pm = 1/2$ can be mapped to a theory of massive Luther-Emery fermion with a chemical potential disorder[13], known to be Anderson localized for all the eigenstates[58]. It can be further inferred that the physical state is a gapless insulator due to the structures of density and current operators in bosonization/refermionization[13]. Away from $K_\pm = 1/2$, the refermionized theory becomes interacting and is no longer exactly solvable. For $K_\pm < 1/2$, the backscattering is enhanced due to the additional repulsive interaction[59–61] so the localization is stable. For $K_\pm > 1/2$, the localization grows less stable as increasing $K_\pm$, and the critical point ($K_\pm = 3/4$) is obtained from bosonization analysis. The localizing mechanism here gives a non-monotonic dependence in Δ with the strongest localization when Δ is comparable to $\delta Q_\pm$[13].

B. Inter-edge localized state

When both the symmetric and anti-symmetric sectors are localized ($K_+, K_- < 3/4$), the edge state breaks TR symmetry spontaneously. We can define pseudospin operators for each edge[13,14] whose finite expectation values indicate TR breaking of the localized states. The pseudospin expectation values in the localized state are random in space and uncorrelated among the two isolated edges. The localized state here can be viewed two localized edges carrying half-charge[13]. The Luther-Emery fermions at $K_+ = K_- = 1/2$ correspond to symmetric or the antisymmetric collective modes of the half-charge excitations among two edges. Importantly, this inter-edge instability ($K_+, K_- < 3/4$) dominates over the leading intra-edge instability ($K < 3/8$)[14,15] because the critical interaction strength is weaker (larger Luttinger parameter).

C. Interlocked fluid state

For weaker interactions, there might exist a region such that only one of the inter-edge degrees of freedom is localized. The correlation among two edges is determined by the *remaining* delocalized collective mode. Such correlated states are called interlocked fluids in the studies of one-dimensional Coulomb drag and reflect the Luttinger liquid behavior[44,45,62]. Here, we focus on the Coulomb drag physics among two generically unequal TI edges. This case was not considered in the existing literature.

For two isolated dirty TI edges with different electron densities, both the symmetric and anti-symmetric sectors are similar except $1 < K_- < K_+$ (due to the repulsive inter-edge Luttinger interactions). A negative interlocked fluid can arise when $K_+ < 3/4$ and $K_- > 3/4$ since the symmetric sector is localized. Such a correlated state is described by an anti-symmetric inter-edge collective mode, corresponding to a perfect "negative drag". In two dimensional electronic systems, a perfect negative drag can arise due to inter-layer exciton formation[63,64]. Similarly, a negative drag between two clean one-dimensional systems can also take place when the commensurate condition $|\delta Q_+| < \delta Q_c$ ($k_{F1} \approx -k_{F2}$) is finely tuned[39,65]. Here, the interlocked anti-symmetric state is not induced by gapping at commensuration but by localizing the collective degrees of freedom. This localization-driven anti-symmetric interlocked fluid is also complementary to the early study for incommensurate clean quantum wires[66]. The phase diagram of the two dirty TI edges with different densities is summarized in Fig. 1.

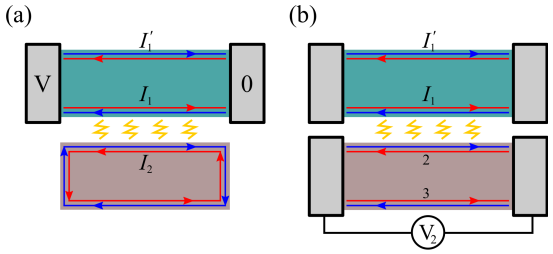

FIG. 2. (a) The proposed experimental setup[39] ("edge gear") for studying the inter-edge correlated states. The top TI is attached to two external electrodes which result in two separated edges carrying current I_1 and I_1'; the bottom TI forms a close edge loop with a current I_2 (but without a voltage drop). The two proximate edge states (carrying currents I_1 and I_2) interact via inter-edge Coulomb interactions. As discussed in the main text, the two terminal conductance on the top TI encodes the information of the inter-edge correlated states. (b) The standard Coulomb drag experiment in the lateral geometry as a comparison.

As a comparison, for two clean TI edges with the same electron density ($k_{F1} = k_{F2}$), the inter-edge interaction $\mathcal{S}_{U,-}$ [given by Eq. (5c)] becomes to a commensurate backscattering term ($\delta Q_- = 0$) that gaps out the anti-symmetric mode for $K_- < 1$[44,45] at zero temperature. The system therefore develops a symmetric interlocked fluid dictating a perfect positive drag[39,44,45]. In the presence of disorder, the symmetric interlocked fluid remains stable as long as $K_+ > 3/4$. The fully gapped anti-symmetric mode becomes to a gapless localized state because the long range order is unstable against *random field* disorder in one dimension[13,57]. For $K_+ < 3/4$, the system develops an inter-edge fully localized state that halts conduction at all.

D. Stability of interlocked fluid states

In Ref. 67, the stability of a perfect drag against the single-particle impurity scattering was investigated. The impurity scattering with in a quantum wire can hybridize the symmetric and anti-symmetric collective modes. As a consequence, the perfect drag is only stable above certain temperature scale set by disorder scattering[67]. Here, we repeat the same analysis for drags among two helical Luttinger liquids.

Due to the TR symmetry, the single-particle backscattering (e.g., $L_1^\dagger R_1$) is not allowed. Therefore, we consider the TR symmetric impurity two-particle backscattering interaction[14,68] as follows:

$$\hat{H}_{\rm imp} = \sum_{a=1,2} W_a \left[L_a^\dagger(0+\alpha)L_a^\dagger(0)R_a(0)R_a(0+\alpha) + \text{H.c.}\right], \tag{6}$$

where W is the strength of impurity interaction and a point splitting with the ultraviolet length α is performed. The corresponding bosonic action is

$$\begin{aligned}\mathcal{S}_W =& \sum_{a=1,2} \tilde{W}_a \int d\tau \, \cos\left[4\theta(\tau, x=0)\right] \\ =& \tilde{W}_1 \int d\tau \, \cos\left[2\sqrt{2}\left(\Theta_+ + \Theta_-\right)\right] \\ &+ \tilde{W}_2 \int d\tau \, \cos\left[2\sqrt{2}\left(\Theta_+ - \Theta_-\right)\right]\end{aligned} \tag{7}$$

where $\tilde{W}_a = W_a/(2\pi^2\alpha^2)$. Based on the scaling dimensions[14,68], $\tilde{W}_1$ and $\tilde{W}_2$ become relevant when $K_+ + K_- < 1/2$. These intra-edge interactions are the subleading perturbations because the inter-edge localizaiton happens when $K_\pm < 3/4$. (As a comparison, the clean helical Luttinger liquid drag happens when $K_- < 1$[39].)

To further investigate the stability of the interlocked fluid states, we follow the treatment in Ref. 67. We focus on the antisymmetric interlocked fluid (negative drag) for $K_+ < 3/4$ and $K_- > 3/4$. Then, we assume the symmetric sector is in the semicalssical limit ($K_+ \to 0^+$). In such an approximation, the $\Theta_+(\tau, x)$ can be replaced by a time-independent function $\gamma_+(x)$, and all the contributions from instanton tunnelings between degenerate vacuums are ignored. Enabling the instanton tunneling will make the impurity scattering less relevant, so the semiclassical treatment here can be viewed as "the worst case scenario". The impurity two-particle backscattering interaction is approximated by $\cos(2\sqrt{2}\Theta_- + C)$ where C is an unimportant constant. As a consequence, Eq. (7) becomes relevant when $K_- < 1/2$. This analysis confirms that the antisymmetric interlocked fluid ($K_+ < 3/4 < K_-$) remains stable when the symmetric mode is fully localized. The same stability also applies to the symmetric interlocked fluid due to two helical liquids with the same density for $K_+ > 1/2$.

In conclusion, the intra-edge perturbations do not sabotage the interlocked fluid states among two helical Luttinger liquid, in contrast to the conventional Coulomb drag[44,45] where the stability against the impurity backscattering is only valid for temperatures higher than the scale set by disorder[67]. The stability of drag among helical liquids is a manifestation of the topological protection in the topological insulator edges.

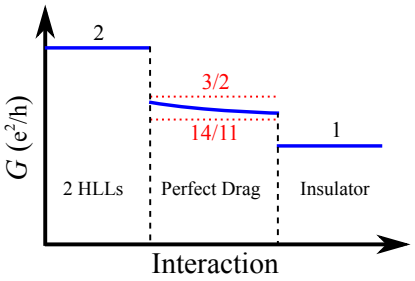

FIG. 3. The two terminal conductance at zero temperature as a function of interaction in the edge gear setup [Fig. 2 (a)]. For sufficiently weak inter-edge interactions, the conductance (in the unit of e^2/h) is 2 as the absence of the bottom close loop TI. In the perfect drag regime, the conductance follows Eq. (8) with an upper bound 3/2 and a lower bound 14/11 (red dotted lines). These bounds guarantee discontinuities of the conductance. For sufficiently strong interactions, two TI edge states become localized insulators. The conductance becomes to 1.

IV. PROPOSED EXPERIMENTAL SETUP

The physics of two isolated TI edges is related to the Coulomb drag experiments[46,47,62,69] in one dimensional systems. We focus on the "edge gear" setup[39] [in Fig. 2 (a)] that detects all the inter-edge correlated states discussed above. We will first focus on infinitely long edges at zero temperature. The corrections due to finite sizes and/or finite temperatures are discussed via existing well-known properties of the localized insulator and Luttinger liquid analysis.

A. Edge gear setup: Results with an infinite long size at zero temperature

The edge gear setup[39] in Fig. 2 (a) contains two isolated TI systems in the lateral geometry. Two TIs are separated via a gap such that two proximate edges can interact via Coulomb force, but the electron tunneling is prohibited. The top TI is connected to two external leads while the bottom TI forms a close edge loop. The two terminal conductance is measured in the top TI system whose value generically encodes the inter-edge correlation.

Firstly, in the absence of any inter-edge interaction, the conductance is $2\frac{e^2}{h}$ (due to two edge channels) independent of the Luttinger parameter[70–72]. For both $K_+, K_- < 3/4$, the inter-edge localized state takes place and makes $I_1 = I_2 = 0$. The conductance is therefore

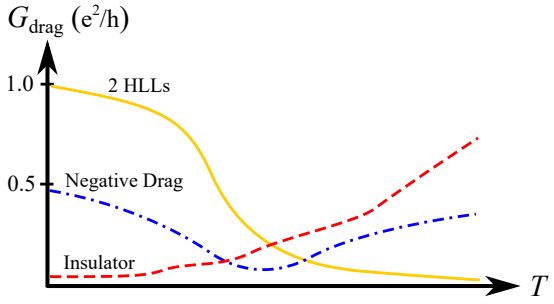

FIG. 4. The sketched temperature dependence of drag conductance in various regimes. $G_{\rm drag} = G - \frac{e^2}{h}$ where G is the two-terminal conductance of edge gear setup. The yellow solid line indicates the two helical liquids regime ($K_+, K_- > 3/4$); the blue dot-dashed line indicates the negative drag ($K_+ < 3/4 < K_-$); the red dashed line indicates the localized regime ($K_+, K_- < 3/4$). The detail features of each curve are explained qualitatively in the main text.

reduced to $\frac{e^2}{h}$ as only the edge with current I_1' is conducting. For the interlocked fluids, the inter-edge interactions induce $I_1 = \pm I_2$ where the positive/negative sign corresponds to the perfect positive/negative drag. The conductance (for both the positive and negative drags)[39] is

$$G = \frac{I_1' + I_1}{V} = \frac{e^2}{h}\left[1 + \frac{1}{1+1/K}\right] \tag{8}$$

which encodes the Luttinger parameter K[73] of the close loop TI edge state. The non-universal conductance varies from $\frac{3}{2}\frac{e^2}{h}$ ($K = 1$, non-interacting limit) to $\frac{14}{11}\frac{e^2}{h}$ ($K = 3/8$, intra-edge instability[14,15]). As plotted in Fig. 3, those bounds ensure two stage conductance "transitions" (discontinuities) when tuning the interaction. We note that Eq. (8) is based on the "Luttinger liquid lead" approximation[39]. For an ideal close loop (infinite coherence time) in the perfect drag regime[74], the conductance is predicted to be $2e^2/h$ as if the close loop was absent.

The only missing ingredient from the edge gear setup is the "sign" (positive/negative) of the perfect drag since the two terminal conductance in Eq. (8) only encodes the electron correlation. A separate measurement (e.g., imaging edge currents via SQUID[75,76]) is required for revealing the parallel/anti-parallel nature of the interlocked fluid states.

B. Edge gear setup: Finite size and finite temperature corrections

Now, we discuss the finite size and the finite temperature corrections. All the localization-driven correlated states predicted in this work require the edge length $L \gg \xi_{\rm loc}$ where $\xi_{\rm loc}$ is the localization length. The drag conductance ($G_{\rm drag} = I_1/V$) can be expressed by $G_{\rm drag} = G_+ + G_-$, where G_+ and G_- are the conductance contributions due to the symmetric and anti-symmetric sectors respectively.

For delocalized modes ($K_\pm > 3/4$), the primary sources of perturbations come from the inelastic scattering due to $\hat{H}_{U,\pm}$. The leading conductance correction is given by $\delta G_\pm = G_\pm - G_{\pm,0} \propto -T^{4K_\pm - 2}$ for $T \ll \Delta/v$[39], where $G_{\pm,0}$ is the conductance at zero temperature. At sufficiently high temperature, we can deduce the conductance via the conductivity of the Luttinger liquid analysis[39]. For $T \gg v|\delta Q_\pm|$, the conductance is given by $G_\pm = \frac{\sigma_\pm}{L} \propto T^{-4K_\pm + 3}$[39], where $\sigma_\pm$ is the conductivity of the symmetric/anti-symmetric sector.

For $K_+ < 3/4$ ($K_- < 3/4$), the symmetric (anti-symmetric) mode becomes localized. In a finite length localized insulator, there exist multiple temperature regimes[78]. For sufficiently high temperatures, the thermal length is smaller than the localization length so the Luttinger liquid analysis can be applied[39,44,45,53]. We summarize the temperature dependence as follows:

$$G_\pm^{\rm loc} \propto \begin{cases} e^{-2L/\xi_{{\rm loc},\pm}}, & \text{for } T \ll T_\pm' \\ e^{-{\rm const}\sqrt{T_{0,\pm}/T}}, & \text{for } T_\pm' \ll T \ll T_{0,\pm} \\ e^{-T_{0,\pm}/T}, & \text{for } T_{0,\pm} \ll T < \delta E_{m,\pm}, \\ T^{-4K_\pm+2}, & \text{for } \delta E_{m,\pm} \ll T \ll \Delta/v \\ T^{-4K_\pm+3}, & \text{for } T \gg \delta E_{m,\pm}, v|\delta Q_\pm| \end{cases} \tag{9}$$

where $\xi_{{\rm loc},\pm}$ is the localization length in the symmetric/anti-symmetric sector, $T_\pm'$ and $T_{0,\pm}$ correspond to the lower and upper bounds of the variable range hopping mechanism[77,78], and δE_m indicates the distance between mobility edge energy and the fermi energy in a finite size 1D insulator. $T_\pm' \equiv v\xi_{{\rm loc},\pm}/L^2$ is determined by setting the optimal hopping length to be the same as the finite edge length L; $T_{0,\pm} \equiv v/\xi_{{\rm loc},\pm}$ corresponds to the typical energy separation in a localized length $\xi_{{\rm loc},\pm}$. For $T \gg \delta E_m$, the localized state is no longer sharply defined. We can treat the backscattering interactions as perturbations with the Luttinger liquid analysis. The standard drag conductivity predicts two high temperature regimes[39,53] similar to the results for $K_\pm > 3/4$. The regime yields $T^{-4K_\pm+2}$ will disappear if $\delta E_{m,\pm} \geq \Delta/v$. We note that the conductance $G_\pm^{\rm loc}$ is at most $\frac{1}{2}e^2/h$.

Combining the results above, we summarize the temperature dependence in the three regimes. All the results are summarized in Fig. 4. In the decoupled helical liquids regime ($K_+, K_- > 3/4$), the measured two-terminal conductance (G_L) is given by[39]

$$G_L(T) = \begin{cases} 2\frac{e^2}{h} - A_1 T^{4K_+-2} - A_2 T^{4K_--2}, & \text{for } T \ll \Delta/v, \\ \frac{e^2}{h} + B_1 T^{-4K_++3} + B_2 T^{-4K_-+3}, & \text{for } T \gg v|\delta Q_\pm|, \end{cases} \tag{10}$$

where $A_{1,2}$ and $B_{1,2}$ are temperature independent constants. The conductance is monotonically decreasing as

increasing T in this regime. The size dependence are absorbed into $A_{1,2}$ and $B_{1,2}$

In the inter-edge localized regime ($K_+, K_- < 3/4$), the conductance is $G_L(T) = \frac{e^2}{h} + G_+^{\rm loc} + G_-^{\rm loc}$ where $G_+^{\rm loc}$ and $G_-^{\rm loc}$ are given by Eq. (9). The highest temperature regime gives a temperature enhancing conductance behavior because $-4K_\pm + 3 > 0$. The conductance is essentially a monotonically increasing function of temperature. The potential non-monotonicity is in the vicinity of $T \sim \Delta/v$ when $1/2 < K_\pm < 3/4$.

In the negative drag regime ($K_+ < 3/4, K_- > 3/4$), the zero temperature conductance of a finite size system is $G_L(0) = G + C\frac{e^2}{h} e^{2L/\xi_{{\rm loc},+}}$ where G is given by Eq. (8) and C is a constant. The temperature dependent conductance is given by

$$G_L(T) = \begin{cases} G_L(0) - D_1 T^{4K_- - 2}, & \text{for } T \ll \Delta/v, \\ \frac{e^2}{h} + \frac{D_2}{T^{4K_+ - 3}} + \frac{D_3}{T^{4K_- - 3}}, & \text{for } T \gg v|\delta Q_+|, \delta E_m, \end{cases} \tag{11}$$

where D_1, D_2, and D_3 are constants. At high temperatures, the D_2 term wins over D_3 term because $4K_+ - 3 < 0 < 4K_- - 3$. The conductance in the negative drag regime is a non-monotonic function in temperature. The non-monotonicity can be understood by the interplay of the localized symmetric mode (monotonically increasing conductance) and delocalized antisymmetric mode (monotonically decreasing conductance).

C. Drag resistivity setup

As a comparison, we discuss the standard "drag resistivity" setup[46,47] as illustrated in Fig. 2 (b). The drag resistance is defined by $R_D = -V_2/I_1$. V_2 is the generated voltage canceling the electromotive force due to the inter-edge interaction. Both the inter-edge localized and the interlocked fluid states tend to develop infinite zero-temperature drag resistivity $\rho_D = R_D/L$ (where L is the length of edge). The sign of the perfect drag can be measured in principle. Meanwhile, the inter-edge localized state also contributes a non-universal sign which is determined by the *weaker* localized inter-edge collective mode. We therefore conclude that there is no simple way to separate inter-edge localized and interlocked fluid states from the standard setup in the zero temperature limit. In addition to the above mentioned issues, the edge 3 in the bottom TI [of Fig. 2 (b)] most likely shorts the system.

V. SUMMARY AND DISCUSSION

We have studied the zero temperature phases in two isolated dirty interacting TI edges. We showed that an inter-edge localized state can generically takes place due to an interplay of TR symmetric disorder and inter-edge interactions. We also predicted that an anti-symmetric interlocked fluid state, producing a negative drag, can arise among two dirty TI edges with different densities. The anti-symmetric interlocked fluid is a consequence of localized symmetric collective mode and delocalized antisymmetric collective mode. Moreover, the interlocked fluids states among two TI edges is founded to be stable down to zero temperature, in contrast to the quantum wire systems where the drag is only valid above some temperature corresponding to disorder scattering[67]. Our study explicitly shows that non-trivial inter-edge correlations can still arise even without commensuration. The zero and finite temperature transport signatures of the edge gear setup[39] are discussed.

We comment on the negative drag between two generically unequal TI edges. This scenario is specific to TI edge states where single particle backscattering is absent, so the negative drag can be viewed as a signature of Coulomb drag among helical Luttinger liquids. The condition of different densities is reminiscent of the experimental observation of negative drag among asymmetric quantum wires[69] whose mechanism has not been concluded yet. Our results might provide a new perspective for understanding the negative drag in one dimensional systems.

In this work, we merely consider sufficiently long TI edges within the standard Luttinger liquid analysis and the linear response theory. The effect of dispersion nonlinearity[79] and the finite electric field response[80] are interesting future directions. The finite close edge loop correction in the edge gear setup [Fig. 2 (a)], potentially generating a resonant feedback for an ac drive, is an interesting topic in the future.

Acknowledgment.– We thank Matthew Foster, Chang-Tse Hsieh, Tingxin Li, Rahul Nandkishore, Leo Radzihovsky, and Zhentao Wang for useful discussions. We are also grateful to Rahul Nandkishore for the useful feedback on this manuscript. This work is supported in part by a Simons Investigator award to Leo Radzihovsky and in part by the Army Research Office under Grant Number W911NF-17-1-0482. The views and conclusions contained in this document are those of the authors and should not be interpreted as representing the official policies, either expressed or implied, of the Army Research Office or the U.S. Government. The U.S. Government is authorized to reproduce and distribute reprints for Government purposes notwithstanding any copyright notation herein.

* YangZhi.Chou@colorado.edu

[1] P. W. Anderson, Phys. Rev. **109**, 1492 (1958).
[2] D. Basko, I. Aleiner, and B. Altshuler, Annals of Physics **321**, 1126 (2006).
[3] I. V. Gornyi, A. D. Mirlin, and D. G. Polyakov, Phys. Rev. Lett. **95**, 206603 (2005).
[4] R. Nandkishore and D. A. Huse, Annual Review of Condensed Matter Physics **6**, 15 (2015).
[5] D. A. Huse, R. Nandkishore, V. Oganesyan, A. Pal, and S. L. Sondhi, Phys. Rev. B **88**, 014206 (2013).
[6] C. L. Kane and E. J. Mele, Phy. Rev. Lett. **95**, 146802 (2005).
[7] C. L. Kane and E. J. Mele, Phy. Rev. Lett. **95**, 226801 (2005).
[8] B. A. Bernevig and S.-C. Zhang, Phys. Rev. Lett. **96**, 106802 (2006).
[9] M. Z. Hasan and C. L. Kane, Rev. Mod. Phys. **82**, 3045 (2010).
[10] X.-L. Qi and S.-C. Zhang, Rev. Mod. Phys. **83**, 1057 (2011).
[11] T. Senthil, Annual Review of Condensed Matter Physics **6**, 299 (2015).
[12] H.-Y. Xie, H. Li, Y.-Z. Chou, and M. S. Foster, Phys. Rev. Lett. **116**, 086603 (2016).
[13] Y.-Z. Chou, R. M. Nandkishore, and L. Radzihovsky, Phys. Rev. B **98**, 054205 (2018).
[14] C. Wu, B. A. Bernevig, and S.-C. Zhang, Phys. Rev. Lett. **96**, 106401 (2006).
[15] C. Xu and J. E. Moore, Phys. Rev. B **73**, 045322 (2006).
[16] M. König, S. Wiedmann, C. Brüne, A. Roth, H. Buhmann, L. W. Molenkamp, X.-L. Qi, and S.-C. Zhang, Science **318**, 766 (2007).
[17] I. Knez, R.-R. Du, and G. Sullivan, Phys. Rev. Lett. **107**, 136603 (2011).
[18] K. Suzuki, Y. Harada, K. Onomitsu, and K. Muraki, Phys. Rev. B **87**, 235311 (2013).
[19] L. Du, I. Knez, G. Sullivan, and R.-R. Du, Phys. Rev. Lett. **114**, 096802 (2015).
[20] T. Li, P. Wang, H. Fu, L. Du, K. A. Schreiber, X. Mu, X. Liu, G. Sullivan, G. A. Csáthy, X. Lin, and R.-R. Du, Phys. Rev. Lett. **115**, 136804 (2015).
[21] F. Qu, A. J. A. Beukman, S. Nadj-Perge, M. Wimmer, B.-M. Nguyen, W. Yi, J. Thorp, M. Sokolich, A. A. Kiselev, M. J. Manfra, C. M. Marcus, and L. P. Kouwenhoven, Phys. Rev. Lett. **115**, 036803 (2015).
[22] E. Y. Ma, M. R. Calvo, J. Wang, B. Lian, M. Mühlbauer, C. Brüne, Y.-T. Cui, K. Lai, W. Kundhikanjana, Y. Yang, M. Baenninger, M. König, C. Ames, H. Buhmann, P. Leubner, L. W. Molenkamp, S.-C. Zhang, D. Goldhaber-Gordon, M. A. Kelly, and Z.-X. Shen, Nature communications **6** (2015).
[23] F. Nichele, H. J. Suominen, M. Kjaergaard, C. M. Marcus, E. Sajadi, J. A. Folk, F. Qu, A. J. Beukman, F. K. de Vries, J. van Veen, *et al.*, New Journal of Physics **18**, 083005 (2016).
[24] B.-M. Nguyen, A. A. Kiselev, R. Noah, W. Yi, F. Qu, A. J. A. Beukman, F. K. de Vries, J. van Veen, S. Nadj-Perge, L. P. Kouwenhoven, M. Kjaergaard, H. J. Suominen, F. Nichele, C. M. Marcus, M. J. Manfra, and M. Sokolich, Phys. Rev. Lett. **117**, 077701 (2016).
[25] F. Couëdo, H. Irie, K. Suzuki, K. Onomitsu, and K. Muraki, Phys. Rev. B **94**, 035301 (2016).
[26] Z. Fei, T. Palomaki, S. Wu, W. Zhao, X. Cai, B. Sun, P. Nguyen, J. Finney, X. Xu, and D. H. Cobden, Nature Physics **13**, 677 (2017).
[27] L. Du, T. Li, W. Lou, X. Wu, X. Liu, Z. Han, C. Zhang, G. Sullivan, A. Ikhlassi, K. Chang, and R.-R. Du, Phys. Rev. Lett. **119**, 056803 (2017).
[28] T. Li, P. Wang, G. Sullivan, X. Lin, and R.-R. Du, Phys. Rev. B **96**, 241406 (2017).
[29] S. Tang, C. Zhang, D. Wong, Z. Pedramrazi, H.-Z. Tsai, C. Jia, B. Moritz, M. Claassen, H. Ryu, S. Kahn, *et al.*, Nature Physics **13**, 683 (2017).
[30] S. Wu, V. Fatemi, Q. D. Gibson, K. Watanabe, T. Taniguchi, R. J. Cava, and P. Jarillo-Herrero, Science **359**, 76 (2018).
[31] L. Fu and C. L. Kane, Phys. Rev. B **79**, 161408 (2009).
[32] F. Zhang and C. L. Kane, Phys. Rev. Lett. **113**, 036401 (2014).
[33] C. P. Orth, R. P. Tiwari, T. Meng, and T. L. Schmidt, Phys. Rev. B **91**, 081406 (2015).
[34] J. Alicea and P. Fendley, Annual Review of Condensed Matter Physics **7**, 119 (2016).
[35] G. Dolcetto, M. Sassetti, and T. L. Schmidt, arXiv preprint arXiv:1511.06141 (2015).
[36] S. Rachel, arXiv preprint arXiv:1804.10656 (2018).
[37] Y. Tanaka and N. Nagaosa, Phys. Rev. Lett. **103**, 166403 (2009).
[38] V. A. Zyuzin and G. A. Fiete, Phys. Rev. B **82**, 113305 (2010).
[39] Y.-Z. Chou, A. Levchenko, and M. S. Foster, Phys. Rev. Lett. **115**, 186404 (2015).
[40] R. A. Santos and D. B. Gutman, Phys. Rev. B **92**, 075135 (2015).
[41] R. A. Santos, D. B. Gutman, and S. T. Carr, Phys. Rev. B **93**, 235436 (2016).
[42] N. Kainaris, I. V. Gornyi, A. Levchenko, and D. G. Polyakov, Phys. Rev. B **95**, 045150 (2017).
[43] V. Kagalovsky, A. Chudnovskiy, and I. Yurkevich, arXiv preprint arXiv:1804.09675 (2018).
[44] Y. V. Nazarov and D. V. Averin, Phys. Rev. Lett. **81**, 653 (1998).
[45] R. Klesse and A. Stern, Phys. Rev. B **62**, 16912 (2000).
[46] A. G. Rojo, Journal of Physics: Condensed Matter **11**, R31 (1999).
[47] B. N. Narozhny and A. Levchenko, Rev. Mod. Phys. **88**, 025003 (2016).
[48] T. L. Schmidt, S. Rachel, F. von Oppen, and L. I. Glazman, Phy. Rev. Lett. **108**, 156402 (2012).
[49] N. Kainaris, I. V. Gornyi, S. T. Carr, and A. D. Mirlin, Phys. Rev. B **90**, 075118 (2014).
[50] T. Giamarchi, *Quantum physics in one dimension* (Oxford Science Publications, 2004).
[51] R. Shankar, *Quantum Field Theory and Condensed Matter: An Introduction* (Cambridge University Press, 2017).
[52] V. L. Pokrovsky and A. L. Talapov, Phys. Rev. Lett. **42**, 65 (1979).
[53] G. A. Fiete, K. Le Hur, and L. Balents, Phys. Rev. B **73**, 165104 (2006).
[54] The same critical value for two helical edges was also obtained in[41] where Θ_- is gapped and inter-edge tunneling is allowed. Our model excludes inter-edge tunneling and

represent a different mechanism of localization.
[55] T. Giamarchi and H. J. Schulz, Phys. Rev. B **37**, 325 (1988).
[56] M. P. A. Fisher, P. B. Weichman, G. Grinstein, and D. S. Fisher, Phys. Rev. B **40**, 546 (1989).
[57] Y. Imry and S.-k. Ma, Phys. Rev. Lett. **35**, 1399 (1975).
[58] M. Bocquet, Nuclear Physics B **546**, 621 (1999).
[59] C. L. Kane and M. P. A. Fisher, Phys. Rev. B **46**, 15233 (1992).
[60] K. A. Matveev, D. Yue, and L. I. Glazman, Phys. Rev. Lett. **71**, 3351 (1993).
[61] M. Garst, D. S. Novikov, A. Stern, and L. I. Glazman, Phys. Rev. B **77**, 035128 (2008).
[62] D. Laroche, G. Gervais, M. Lilly, and J. Reno, Science **343**, 631 (2014).
[63] J.-J. Su and A. MacDonald, Nature Physics **4**, 799 (2008).
[64] D. Nandi, A. Finck, J. Eisenstein, L. Pfeiffer, and K. West, Nature **488**, 481 (2012).
[65] S. C. Furuya, H. Matsuura, and M. Ogata, arXiv preprint arXiv:1503.02499 (2015).
[66] T. Fuchs, R. Klesse, and A. Stern, Phys. Rev. B **71**, 045321 (2005).
[67] V. Ponomarenko and D. Averin, Phys. Rev. Lett. **85**, 4928 (2000).
[68] J. Maciejko, C. Liu, Y. Oreg, X.-L. Qi, C. Wu, and S.-C. Zhang, Phys. Rev. Lett. **102**, 256803 (2009).
[69] M. Yamamoto, M. Stopa, Y. Tokura, Y. Hirayama, and S. Tarucha, Science **313**, 204 (2006).
[70] I. Safi and H. J. Schulz, Phys. Rev. B **52**, R17040 (1995).
[71] D. L. Maslov and M. Stone, Phys. Rev. B **52**, R5539 (1995).
[72] V. V. Ponomarenko, Phys. Rev. B **52**, R8666 (1995).
[73] We adopt the "Luttinger liquid lead" approximation[39]. The conductance is determined by the region without inter-edge interaction[39,70–72], so its value depends on K instead of K_+.
[74] B. Horovitz, T. Giamarchi, and P. L. Doussal, arXiv preprint arXiv:1805.00996 (2018).
[75] K. C. Nowack, E. M. Spanton, M. Baenninger, M. König, J. R. Kirtley, B. Kalisky, C. Ames, P. Leubner, C. Brüne, H. Buhmann, *et al.*, Nature materials **12**, 787 (2013).
[76] E. M. Spanton, K. C. Nowack, L. Du, G. Sullivan, R.-R. Du, and K. A. Moler, Phys. Rev. Lett. **113**, 026804 (2014).
[77] N. Mott, Philosophical Magazine **13**, 989 (1966).
[78] Y. Imry, *Introduction to mesoscopic physics* (Oxford University Press on Demand, 2002).
[79] A. Imambekov, T. L. Schmidt, and L. I. Glazman, Rev. Mod. Phys. **84**, 1253 (2012).
[80] T. Nattermann, T. Giamarchi, and P. Le Doussal, Phys. Rev. Lett. **91**, 056603 (2003).